Journal of Power Sources 468 (2020) 228369

Contents lists available at ScienceDirect

Journal of Power Sources

journal homepage: www.elsevier.com/locate/jpowsour

Perspective

Understanding capacity fading mechanism of thick electrodes for lithium-ion rechargeable batteries

Kyu-Young Park [a,1], Ji-Won Park [a,1], Won Mo Seong [a], Kyungho Yoon [a], Tae-Hyun Hwang [a], Kun-Hee Ko [a], Ju-Hyeong Han [b], Yang Jaedong [b], Kisuk Kang [a,c,d,*]

[a] Department of Materials Science and Engineering, Research Institute of Advanced Materials (RIAM), Seoul National University, Gwanak-ro 599, Gwanak-gu, Seoul, 151-742, Republic of Korea
[b] SDI R&D Center, Samsung SDI Co., LTD, 130 Samsung-ro, Yeongtong-gu, Suwon-si, Gyeonggi-do, 16678, Republic of Korea
[c] Center for Nanoparticle Research, Institute for Basic Science (IBS), Seoul National University, Gwanak-ro 599, Gwanak-gu, Seoul, 151-742, Republic of Korea
[d] Institute of Engineering Research, College of Engineering, Seoul National University, 1 Gwanak-ro, Gwanak-gu, Seoul, 151-742, Republic of Korea

HIGHLIGHTS

- Cycle degradation issue in thick electrode under high current density.
- The mass transport limitation gets worse as the cycle progresses.
- Permanent mechanical and chemical damages occur at the top layer of the thick electrode.
- A comprehensive cycle degradation model of the thick electrode is provided in this study.

ARTICLE INFO

Keywords:
Lithium-ion batteries
Layered transition metal oxide
Thick electrode
Reaction inhomogeneity
Capacity fading

ABSTRACT

The use of thick electrodes with high-loading density of active material is one of the most practical strategies to increase the volumetric/specific energy density of lithium-ion battery, while taking advantage of the current electrode chemistry. However, their use is accompanied by serious deterioration of electrochemical performance, especially exhibiting poor capacity retention with low power capability. Here, the degradation behavior of the $LiNi_{0.6}Co_{0.2}Mn_{0.2}O_2$, one of widely adopted cathodes, is comparatively investigated under high loading levels as high as 28 mg cm^{-2} over the extended cycling. It is revealed that the charge transport limitation is cumulatively dominated by the lithium ionic diffusion rather than the electronic conduction in the thick electrode. More importantly, as the cycle proceeds, the thick electrode gets exposed to a serious reaction inhomogeneity because of the negative feedback between the accumulated ion transport limitation and locally increasing resistance. It leads to the generation of current hot spot in the electrode and the corresponding local material degradation, which further inhibit the charge transport, resulting in unavoidable capacity fading. This finding proposes that rational electrode architecture detouring the hot spot generation needs to be considered with respect to the ion transport and the electrode material degradation toward the high-loading electrodes.

1. Introduction

Recent advances in lithium-ion batteries have continuously increased their energy density per volume, weight and cost, accelerating the market penetration of electric vehicles (EVs) [1,2]. The newly developed active materials have contributed to increasing the energy density of conventional lithium-ion batteries, endeavoring to bring the driving mileages of EVs closer to that of internal-combustion-engine-based vehicles. For example, the Ni-rich layered oxide cathodes could partly overcome the limited capacity of the traditional $LiCoO_2$ cathodes, and help approach the theoretical limit of the conventional layered $LiMO_2$ electrode (~280 mAh g^{-1}, M = transition metal) [3,4]. As new electrode chemistry, lithium-rich transition metal oxide cathode materials have been under intensive scrutiny

* Corresponding author. Center for Nanoparticle Research, Institute for Basic Science (IBS), Seoul National University, Gwanak-ro 599, Gwanak-gu, Seoul, 151-742, Republic of Korea.
E-mail address: matlgen1@snu.ac.kr (K. Kang).
[1] These authors contributed equally.

https://doi.org/10.1016/j.jpowsour.2020.228369
Received 27 March 2020; Received in revised form 5 May 2020; Accepted 15 May 2020
Available online 11 June 2020
0378-7753/© 2020 Elsevier B.V. All rights reserved.

seeking for a higher energy density beyond the conventional $LiMO_2$ electrode. And, it was demonstrated that an unprecedentedly high capacity can be potentially achieved from the unique anion redox in the lithium-rich oxides [5,6]. While the continuous optimizations of active materials are in progress, the practical energy densities of battery packs still do not meet the demands of long-distance driving of EVs from both gravimetric and volumetric aspects. Further discovery of new electrode materials is expected to enhance the performance of the current lithium-ion batteries, however, the adoption of new chemistry in the manufacturing of lithium-ion batteries is yet far from the immediate reality.

An alternative course to maximize the practical energy density is to minimize the inactive components in the electrode while employing traditional electrode chemistries. Indeed, non-active components, such as current collectors and separators, account for at least ~20% of the total volume or weight of the commercialized battery packs [7]. Therefore, doubling the loading density of active materials could result in an actual capacity increase of approximately 10%–15% per battery. In this respect, a recent report demonstrated that a remarkably high areal capacity could be achieved from the thick electrode by employing carbon nanotube network in the electrode [8]. In addition, the extensive analyses have shown that practical factors such as electrode loading, electrolyte amount and foil thickness are critical in achieving the realistic high energy density [9–11]. Nevertheless, the use of thick electrodes with conventional formulation is inevitably linked with the deterioration of electrochemical properties such as the rate capability in particular. Lee et al. reported that $LiNi_{0.8}Co_{0.1}Mn_{0.1}O_2$ cathode with the electrode loading of ~25 mg cm^{-2} was capable of delivering only less than 20% of the theoretical capacity of the active material under a moderate current density of 2C [12]. A 320-μm thick electrode reported by Singh et al. was only useable below a current density of C/2 [11].

Former theoretical and experimental works suggested that this deterioration most likely results from the elongated charge transfer paths of lithium ions in the high-loading electrode [12–16]. Longer ion diffusion in the electrode would increase the charge-transfer resistance, which becomes more severe and problematic under a high current density. In order to maintain the moderate rate capability, many research groups have previously attempted to reduce the overall tortuosity of the electrode to abate the charge transfer paths and keep the desired loading density or areal capacity [17,18]. While some success has been achieved, it has been still a tremendous challenge to secure sufficiently high power-capability for the practical usage. Moreover, a complicated issue for thick electrodes is that the rate capability is coupled with the capacity retention. In many prior studies, a feasible cycle retention was achieved for a thick electrode only under low current density (~C/5) for short-term cycles (<50 cycles) [12,19,20]. And, even though relatively high-power density seems to be displayed for the initial cycles, the capacity retention over extended cycles is significantly affected by the high-loading of the electrode, as will be discussed in detail later. However, so far, this inferior cycle retention of the thick electrode has not been dealt with systematically. More fundamental understanding is required to elucidate the accelerated degradation behaviors of thick electrodes in correlation with the current density to expedite the practical employment of the thick electrode.

In this work, we systemically investigated the underlying capacity fading mechanism of thick electrodes over extended cycles for $LiNi_{0.6}Co_{0.2}Mn_{0.2}O_2$ cathodes. Through the comparisons of electrodes with different loading levels, it was observed that thick electrodes suffer from the significant reaction inhomogeneity aggravating with cycle number, whereas the conventional electrode maintains the reaction homogeneity even after 100 cycles, as verified by laser-induced breakdown spectroscopy (LIBS) and X-ray diffraction analyses. Moreover, severe particle destruction and formation of byproducts were detected selectively at the top layer of the thick electrode after cycles as a result of the reaction inhomogeneity. Based on the findings, we propose a comprehensive model, including not only determining limiting factor but also mechanical damages and surface chemical changes along the electrode depth, regarding the cycle degradation of the thick electrode. The degradation is initialized by (i) the slightly elongated lithium-ion diffusion route in the electrode, (ii) accompanied by selectively cumulative side reactions, and (iii) followed by the reaction inhomogeneity that becomes severe with negative feedback between the altered tortuosity and side reactions. Eventually, local current hot spots are formed at the electrode, leading to the degradation of the active material. These observations would aid in identifying potential solutions to bottlenecks in employing high-loading thick electrodes toward the high-energy-density batteries with the long-term cyclability.

2. Experimental

2.1. Electrode preparation and electrochemical analysis

To prepare the electrode, $LiNi_{0.6}Co_{0.2}Mn_{0.2}O_2$ powder (provided by Samsung SDI), Denka carbon black, and Polyvinylidene fluoride (PVDF) were mixed in a weight ratio of 97:1.5:1.5 and added to *N*-Methyl-2-pyrrolidone (NMP, anhydrous, 99.5%, Aldrich). After this mixture was homogenized into a slurry, it was coated onto aluminum foil using the doctor-blade method, dried for 20 min in a 120 °C convection oven, and pressed by a roll-pressing machine. Coin-type half cells (CR2032, Wellcos) were assembled using the composite electrode as the cathode, lithium metal as the anode, a glass fiber filter (GF/F) separator, and 1 M $LiPF_6$ in ethylene carbonate/dimethyl carbonate (EC/DMC, 1:1 v/v, PanaX Etec) as the electrolyte. Galvanostatic measurements of the charge/discharge of half-cells were conducted within the voltage range of 2.8–4.3 V with a current density of 150 mA g^{-1} (~1C) at 25 °C using a multichannel potentio-galvanostat (WBCS-3000, Wonatech, Korea). EIS analysis was conducted after the half-cell was charged to 4.3 V every 20 cycles. A sine-modulated AC potential of 10 mV was applied in the frequency range of 200 kHz to 5 mHz.

2.2. Chemical composition analysis

The state of charge (SOC) inhomogeneity was examined using LIBS (J200, Applied Spectra). In employing LIBS, a high-power laser was exposed to a sample to transform it into the plasma state and analyze the elements. The plasma-state material returns to the ground state, emitting characteristic wavelengths of light. The difference in wavelengths for each element allows element species in the material to be identified and quantitatively measured. The spot size of LIBS is approximately 30–200 μm, which was appropriate for observations at the electrode level. We used a wavelength of 266 nm with 11.25 and 17.25 mJ for the standard and thick electrodes, respectively. The cycled cells were immediately disassembled, and the electrodes were retrieved and wiped out within 1 min to prevent the possible re-distribution of lithium ions in the electrode before the LIBS measurement.

2.3. Structural analysis of the electrodes

The morphology of the active materials was observed using scanning electron microscopy (SEM; SU70, Hitachi, and SUPRA). When observing the active particles near the current collector, the electrode materials on the top side were removed using Kapton tape; the top side of the remaining electrode was then examined. The extent of electrolyte decomposition was determined using X-ray photoelectron spectroscopy (XPS; Sigma Probe, Thermo Fisher Scientific, U.K). The binding energy was referenced to the C 1s peak at 284.5 eV. The electrodes were further analyzed using X-ray diffraction (XRD; D2 PHASER, Bruker, Bremen, Germany) with Cu-Kα radiation ($\lambda = 1.54178$). Before collecting the XRD pattern, we evaluated the penetration depth of X-rays using a thin electrode and concluded that the maximum depth is approximately 35 μm (Fig. S1.). This XRD depth represents either less than half of the standard electrode (~70 μm) or nearly one-third of the thick electrode

(~100 μm). To characterize the active particles near the separator, the top side of the electrode was analyzed. For the XRD measurement of the current-collector side, the upper layer of the electrode was carefully peeled off using the taping method until the high peaks of Al were clear.

3. Results and discussion

3.1. Capacity retention of high-loading electrodes

In order to evaluate the effect of the high-loading on the electrochemical performance, we prepared the standard electrode with the commercial loading level of 20 mg cm^{-2} employing $LiNi_{0.6}Co_{0.2}Mn_{0.2}O_2$ (so called NCM622) as a reference, and the thick electrode with 40% higher loading density, *i.e.* 28 mg cm^{-2}. The densities of the electrodes after the preparation process were carefully controlled within the range of 2.8–2.9 mg cm^{-3} to ensure the identical porosity and the electric wiring effect in each electrode for a fair comparison [15,17,21]. Fig. 1a and Fig. 1b depict the cross-sectional image of the two electrodes with ~70 and ~100 μm thick, respectively, which proportionally correspond to the intended loading density, confirming that the electrode densities of the two are almost identical. In addition, computed tomography also showed that both electrodes have a similar porosity of 25% regardless of the thickness (See Fig. S2.). Each electrode was assembled in the coin-type lithium cell, and the specific capacity retention was examined under the practically important current density of 150 mA g^{-1} corresponding to ~1C, as presented in Fig. 1c. The major finding in the comparative cycle test was that the capacity retention of the electrode significantly decreases with the active loading density even by the 40% increase from the commercial loading level. After 100 cycles, the thick electrode only retained 36% of the initial capacity (~56 mAh g^{-1}), whereas the standard electrode exhibited 76% capacity retention (~124 mAh g^{-1}). When considering the areal capacity, the capacity retention of the thick electrode appeared to be even more inferior to that of the standard electrode. The initial areal capacity of the thick electrode was approximately 4.2 mAh cm^{-2}, which is higher than that of the standard electrode (3.0 mAh cm^{-2}); however, it plummets below 1.5 mAh cm^{-2} after 100 cycles, which becomes lower than that of the standard electrode (see Fig. 1d). These results clearly indicate that the capacity retention gets severely deteriorated simply by the high loading of the electrode even with the same cathode chemistry. It is also interesting to note that at the initial cycles, the capacity retention at 1C is comparable to each other, indicating the similar power density of the thick electrode to that of the standard electrode, however, it gets progressively aggravated with extended cycles. It implies that the seemingly comparable power capability during the initial cycles does not reflect the efficacy of the thick electrode.

In elucidating the inferior electrochemical performance observed, we note that thick electrodes are likely to suffer from the kinetic limitations that arise from the finite mobility of charge carriers either dominated by lithium ion transport or the electronic resistance build-up along the electrode (*e.g.* electron transport) during the electrochemical reaction. And, in each case, there will be distinct spatial distribution of the reaction front, assuming that the major supply of the electrons and lithium ions to the electrode takes place from the interface of the electrode/current collector and that of the electrode/electrolyte, respectively, as schematically illustrated in Fig. 2a and Fig. 2b, [13,14]. For the ion-transport limitation circumstance, the active electrode material particles near the current collector are prone to be less utilized in the electrochemical reaction because they require the longest lithium ion path from the electrode/electrolyte interface (Fig. 2a). And, the region near the electrode/electrolyte interface, *i.e.* top layer of the electrode, would be ready for the electrochemical reaction with the sufficiently fast supply of both lithium ion and electron even at a high current density. In the extreme case, the bottom layer electrode may remain idle during the cycling. On the contrary, for the electron transport limiting case, as illustrated in Fig. 2b, the active particles near the electrode/electrolyte interface would suffer from the largest electronic resistance build-up from the current collector and become inaccessible for the electrochemical reaction within the certain voltage cutoff, while the bottom region would be more electrochemically active.

Bearing this in mind, we attempted to monitor the distinct spatial distribution of the reaction front, if any, by quantitively measuring the local SOCs in the electrode in various charge and discharge conditions. The local SOCs were determined along the electrode thickness by

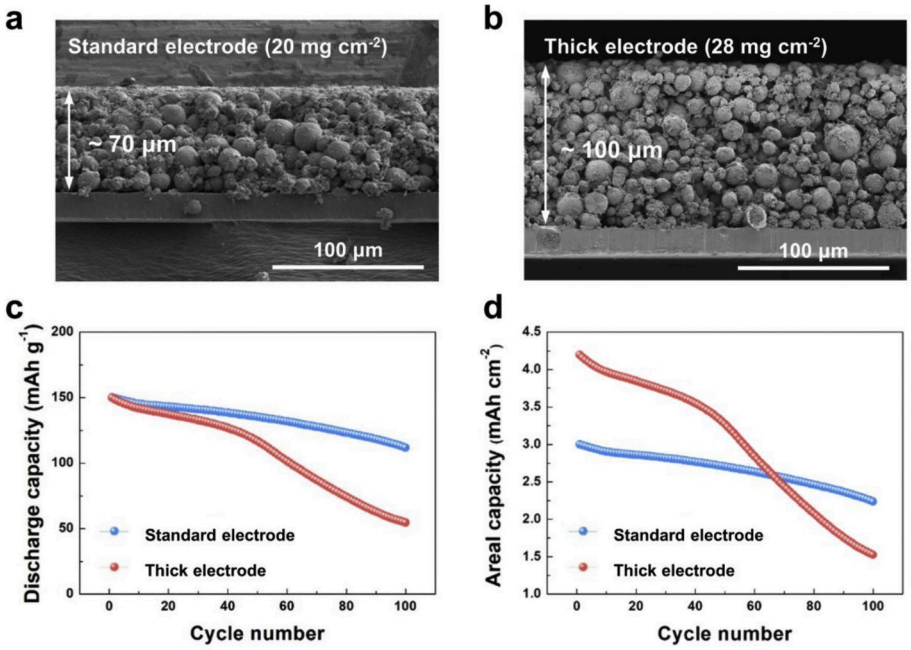

Fig. 1. Cross-sectional SEM images of (a) standard and (b) thick electrodes. Comparison of cycle life of standard (blue) and thick (red) electrodes in terms of (c) specific discharge capacity and (d) areal discharge capacity. The cells were cycled with a current density of 1C within a voltage range of 2.8–4.3 V (*vs.* Li/Li^+). (For interpretation of the references to color in this figure legend, the reader is referred to the Web version of this article.)

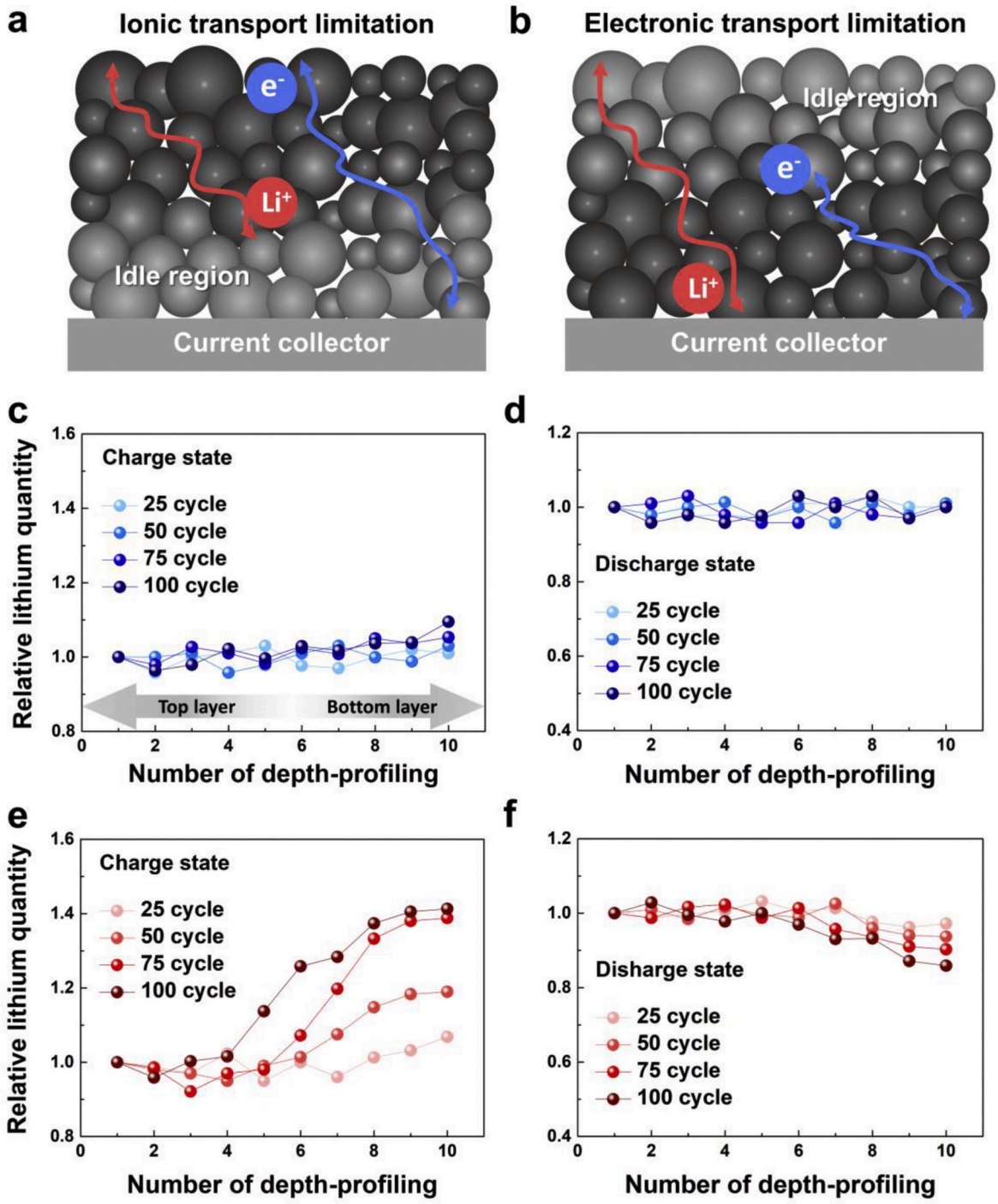

Fig. 2. Schematic illustration of limiting factors in the charge transfer: (a) lithium ions and (b) electrons in a thick electrode. The black balls represent the active particles of the battery electrode. LIBS results of normalized lithium composition deviations every 25 cycles along the electrode depth for (c) the end-charge and (d) end-discharge states of the standard electrode and (e) the end-charge and (f) end-discharge states of the thick electrode.

comparatively tracing the lithium contents with the depth-profiling using the laser-induced breakdown spectroscopy (LIBS). LIBS analysis was particularly suitable for the lithium elemental analysis because of its high sensitivity to the lithium spectra, as shown in Fig. S3a. In our experiment, we set the energy level of LIBS for the depth-profiling on a scale of several micrometers with the adjustable detection area (30–200 μm), which could probe a depth area corresponding to 10% of the thick electrode per measurement, such that after 10 measurements, the bottom bare current collector was exposed (see Fig. S3b. The details of the LIBS measurement are provided in the experimental section). Using these features, we measured the change in the lithium composition along the height in the thick electrode for both end-charge and end-discharge states in every 25 cycles, as presented in Fig. 2c–f. In the figure, we normalized the relative amount of lithium content (*y*-axis) based on the response intensity of the first measurement (*i.e.,* the top layer region) for each depth-profiling data set. In the *x*-axis, a tenth cross-sectional information on the electrode was recorded, where the numbers of 1–10 represent the number of depth-profiling conducted from the top layer, thus the higher number displays the properties of the region closer to the current collector. Fig. 2c and d depict the lithium

distribution along the height in the standard electrode, which indicates the relatively uniform SOCs for all the cycles regardless of the charge and discharge states. It suggests that the electrochemical reaction in the standard electrode occurs homogenously over the entire electrode geometry for the cycles even at 1C rate. However, it was found that significant deviations in the lithium composition are present in the thick electrode from the top to the bottom layer, which becomes more obvious with the cycle number. In Fig. 2e, it was observed that the distribution of SOCs in the electrode is relatively uniform until 25 cycles, however, the deviation begins to kick off from the 50th cycle and it gets severe after 75 cycles, which interestingly agrees to the cycle number where the significantly faster cycle degradation begins to occur in Fig. 1c and d. Noteworthy is that the relative lithium composition is substantially higher at the bottom layer at the end-charge state. It signifies that the charging reaction could not be completed in the electrode near the electrode/current collector interface, which is observed more evidently after longer cycles. Fig. 2f presents the similar set of the data at the end-discharged states, which consistently show that the relative lithium inhomogeneity increases with the cycles. The degree of the non-uniformity, nevertheless, appears to be notably weaker than the case of the end-charge state. However, it needs to be reminded that the discharge process begins with the charged state which already contains the prior significant inhomogeneity, showing much less lithium contents in the top layer. It suggests that much faster lithium content recovery took place in the top layer during the discharge, indicating the significant reaction inhomogeneity in the electrode. Indeed, when we repeated the end-discharge experiment after the electrode was slowly charged to reach a sufficiently uniform charged state, the LIBS results confirmed similarly severe lithium inhomogeneity in the discharge state, as observed in Fig. S4. This observation of SOC variations in the thick electrode suggests that the active electrode particles near the electrolyte is more actively charged and readily discharged than the one near the current collector, strongly supporting that the charge-transfer limitation in the cycled thick electrodes is likely from the lithium ion transport.

The reaction inhomogeneity in the thick electrode could be further verified by XRD by selectively probing the top and bottom layers of the electrodes at every 25 cycles for both end-charge and end-discharge states, as presented in Fig. 3. The full spectra of the XRD along with the calculated lattice parameters are provided in Fig. S5 and Table S1, respectively, in the supplementary information. Fig. 3a and b display the magnified picture of the XRD patterns of the top and bottom regions of the standard electrode. It shows that there is no apparent difference in the peak positions between the two regions during the initial cycles. In the later cycles, the difference becomes slightly bigger, but remains comparatively minor, in consistent with the results of LIBS. Considering the lattice parameters tabulated in Table S1, it is estimated that the SOC difference between the top and bottom region of the standard electrode is less than 5% even after 100 cycles regardless of the charge/discharge states. Fig. 3c also confirms that the difference in the SOCs between the two regions remains negligible with the cycle numbers for both end-charge and end-discharge states, indicating of only small inhomogeneity in the standard electrode after cycles. On the contrary, a clear mismatch between the peak positions was observed for the thick electrode, which was particularly substantial for the samples cycled over 50 times. In Fig. 3d, the (108) and (110) peaks became more split at the top region of the electrode, and the (113) peak noticeably shifted to the right compared with that of the bottom region at the charged state. For the samples in the discharged state (Fig. 3e), a similar trend was observed; the top layer of the active materials exhibited notably lower SOC states than the bottom part. Quantitative analysis of the SOCs in Fig. 3f illustrates that the bottom layers in the thick electrode are far more deviated from the intended SOCs, showing the substantial reaction inhomogeneity. The SOCs at the end-charge and end-discharge states appear to be even converging with cycles particularly for the bottom

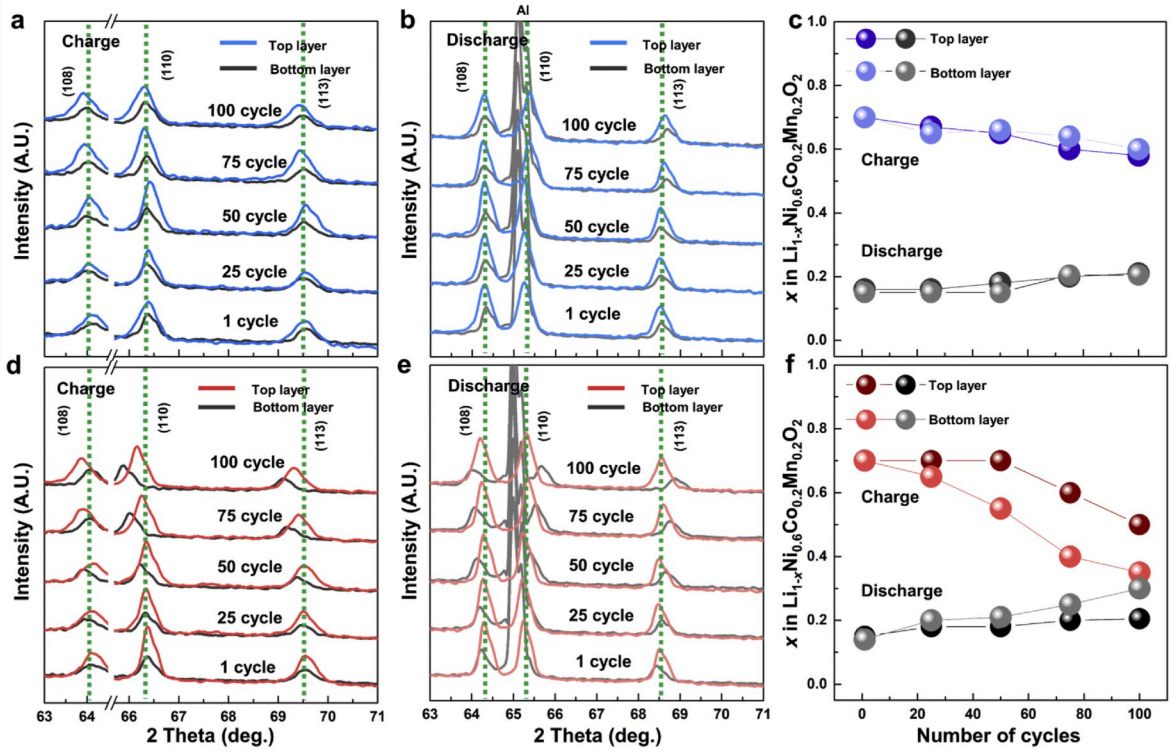

Fig. 3. XRD patterns of cycled standard electrodes for (a) the end-charge and (b) end-discharge states with (c) SOC changes for every 25 cycles for 100 cycles. XRD patterns of (d) the end-charge, (e) end-discharge states and (f) SOC changes of thick electrodes for every 25 cycles for 100 cycles. The black lines represent the bottom layer of the electrode, and the colored lines represent the top layer of the electrode. Al peaks are observed too strong on the patterns of the separator sides at near 65°, thus removed in the plot when possible. Expected SOCs of top and bottom regions from calculated lattice parameters [34]: The colored and black points represent the charged and discharged state after the cycles, respectively.

part of the electrode. At around the 100th cycle, the bottom part close to the current collector no longer participates in the electrode reaction, remaining at the same SOC regardless of the charge and discharge. It implies that as cycling progresses, only the top layer of the thick electrode is utilized for the electrochemical reaction, while the bottom layer remains idle. Considering the XRD penetration depth (Fig. S1) and the areal capacity of the electrode, more than 50% of the capacity is delivered from less than one-third of the thick electrode, *i.e.* top layer.

3.2. Current hot-spot formation and material degradation

The LIBS and XRD results clearly demonstrate that the main kinetic limitation arises from the insufficient lithium-ion transport within the thick electrode. As a result, serious SOC inhomogeneity is generated along the electrode depth due to its limited mass transport issue; the top region of the electrode majorly experiences the electrochemical reaction, whereas the bottom region remains idle, and it gets aggravated over cycles. This implies that at a given areal current density applied, the top layer of the thick electrode would be gradually exposed to a considerably higher effective current density in later cycles, *i.e.*, serving as current hot spots. It is generally accepted that a higher current density can lead to serious damage of the active materials, such as the formation of micro-cracks or irreversible local phase transformation [22–25]. Since the local high current density creates a steep lithium gradient inside the secondary particle, it can engender a large stress field within the particle, breaking up the particles with new exposing surfaces, which continuously produce thick organic surface layers [22,24,26,27]. These undesired side reactions, which build up gradually on the materials, eventually give rise to a high charge-transfer resistance in the electrode, leading to degradation of the cell [26,27].

We also found that the top layers of the thick electrode were selectively and more significantly degraded than the bottom region after cycles, with respect to the morphology and surface nature as verified by SEM and XPS analysis. Fig. 4a–d presents the morphologies of the secondary active particles after 100 cycles at the top and bottom regions of the standard and thick electrodes, respectively. It is shown that the standard electrode did not exhibit noticeable morphology changes in either the top (Fig. 4a) or bottom region (Fig. 4b), indicating the robustness over cycles. On the contrary, it was clearly observed that many of secondary particles in the top layer of the thick electrode contain micro-scale cracks, and some of them have already broken apart in Fig. 4c. However, the particles at the bottom region near the current collector remained intact (Fig. 4d), suggesting that the top layer of the thick electrode had selectively underwent a significant degradation. The degradation of the top electrode region could be further confirmed by XPS measurement probing the surface nature of the secondary particles containing organic byproducts, as presented in Fig. 4e–h. The characteristic carbon peaks are detected in the C 1s spectra for all the samples after cycles with the deconvoluted peaks at 289, 286, and 284.5 eV, corresponding to C═O, C–O, and C–C bonding, respectively. The C–C bonding at 284.5 eV is considered a fingerprint of carbon conducting agents, and the other peaks are attributed to organic byproducts from the electrolyte decomposition deposited on the electrode [28]. Negligible differences in the XPS spectra were observed between the top and bottom regions of the standard electrode (Fig. 4e and f). However, notable discrepancies were observed for the thick electrode, as shown in Fig. 4g and h. The peak intensities of the C═O and C–O bonds from the top region were substantially greater than those for the bottom, indicating that larger amounts of organic byproducts were formed on the top region of the thick electrode. It agrees with the previous works that the electrode material with considerable micro-crack formation triggers the build-up of the thick organic surface layers, increasing the overall impedance of the electrode [22,24,26,27]. Indeed, it was also found that the impedance of the thick electrode increases more rapidly than that of the thin electrode with cycles from the electrochemical impedance spectroscopy (EIS) (see Fig. S6), which is consistent with the faster degradation behavior of the thick electrode. These observations indicate that the development of severe current hot spots occurs particularly at the top layer of the thick electrode and it accompanies side reactions during the repeated electrochemical cycles, contributing to the degradation of the cell.

3.3. Capacity fading mechanism of thick electrodes

Based on the findings in this work, we propose a model for the accelerated capacity fading occurring in high-loading electrodes. During the initial stage of the cycle, the electrochemical reaction takes place in a relatively uniform manner throughout the thick electrode (Fig. 5a) without the serious concentration polarization issue. However, the limited transport of lithium ions within the electrode gradually results in the inhomogeneous electrochemical reaction particularly separating the top and bottom region of the thick electrode, meaning that the IR drop

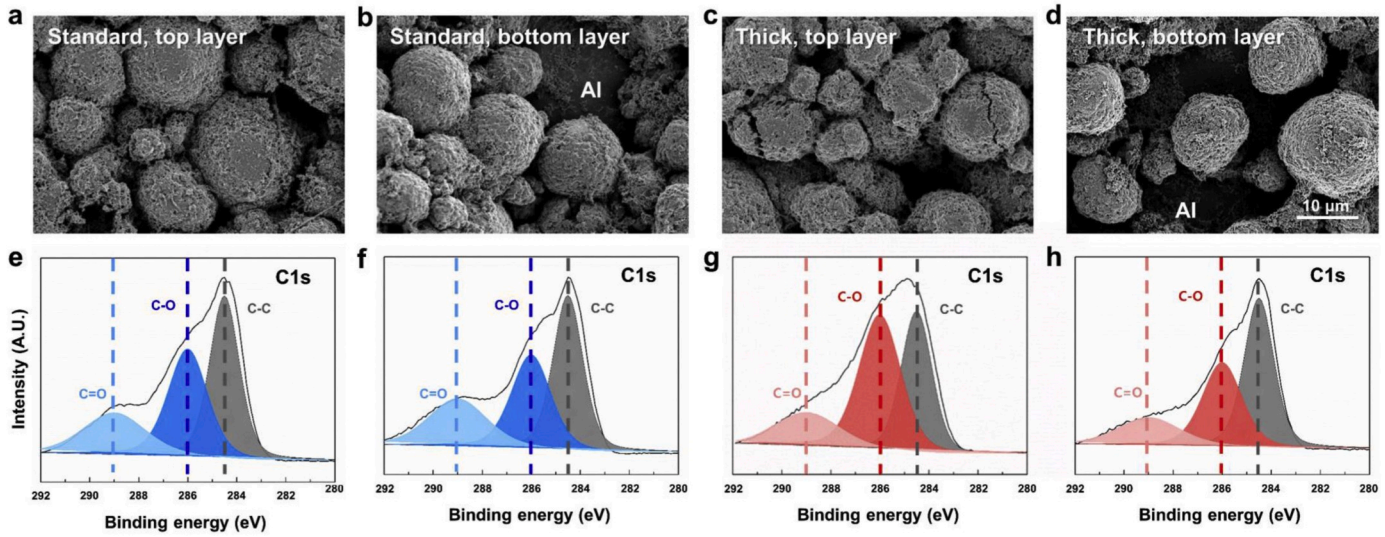

Fig. 4. SEM images of secondary particles after 100 cycles: (a) top layer and (b) bottom layer of standard electrode, (c) top layer and (d) bottom layer of thick electrode. The bottom layer images show the Al current collector in the background. XPS bonding signals of electrolyte decomposition by-products after 100 cycles: (e) top layer and (f) bottom layer of standard electrode, (g) top layer and (h) bottom layer of thick electrode.

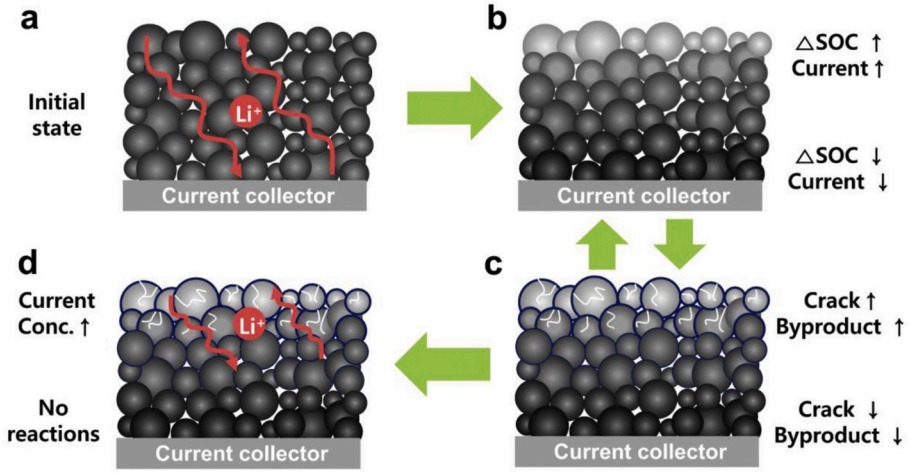

Fig. 5. Schematic illustration of capacity fading mechanism in the thick electrode: (a) intact thick electrode at initial cycling, (b) appearance of SOC/local effective current density differences in thick electrode after cycles, (c) unevenly formed cracks and byproducts on active particles, (d) thick electrode after long-term cycling.

and concentration polarization are not trivial anymore in the thick electrode. Accompanying side reactions and repeated charge/discharge lead to a further increase in the resistance to the transport of lithium ions in the electrode. Subsequently, the top layer of the electrode will be exposed to a higher effective current density, as shown in Fig. 5b. The active particles that receive higher current density will be vulnerable to the electrochemical degradation by mechanical cracks, producing organic surface residues at the newly exposed surfaces. The crack formation and the resulting surface residues increase the complexity of the lithium-ion diffusion path along with the increase in the lithium-ion tortuosity (Fig. 5c). The repeated negative feedback between Fig. 5b and c will reduce the active region available for the electrochemical reactions from the combined tortuosity and transport issues. Eventually, a considerable amount of the active materials in the bottom region cannot participate in electrochemical reactions at all. On the other hand, the particles at the top layer of the electrode get further exposed to more severe effective current density as current hot spots, risking the permanent damage over cycles (Fig. 5d). Our proposed model was further supported by additional experiments provided in supporting information. Using the same standard and thick electrodes, when lithium ions are given with enough time to diffuse such as in constant-current and constant-voltage mode (CCCV), the thick electrode was remarkably less degraded than the case of the conventional galvanostatic cycling even at the same current density. (Fig. S7). The additional constant-voltage charging time could significantly delay the appearance of the current hotspots in the thick electrode, enhancing the cycle performance.

4. Conclusion and perspectives

We systematically investigated the origin of the rapid capacity fading of thick electrodes employing the representative cathode material in a lithium electrochemical cell. While the active weight and thickness of the electrodes differed by only ~40% in our comparative investigation of the standard and thick electrodes, significant electrochemical performance differences were observed for the extended cycles. Compositional and structural analysis using LIBS and XRD revealed the marked increase in the SOC inhomogeneity along the depth of the electrodes as cycling progressed, verifying the limited lithium-ion diffusion in the cycled thick electrode. It was further found that such reaction inhomogeneity became aggravated in later cycles owing to the selective degradation of the secondary active particles and the accumulated resistance to lithium-ion diffusion. As a result, a considerably higher effective current density is applied to the top layer of the electrode, serving as a current hot spot. The severe current concentration eventually causes the formation of serious micro-cracks and side reactions on the active particles, which in turn degrades the cycle stability further.

Understanding of the deterioration mechanism in lithium-ion batteries has been actively pursued in many previous studies with respect to the operating temperature [29], cut-off voltages [30,31] and electrode material types [32,33], which were often found to be closely related with the degradation of active materials. Thick electrodes are also eventually accompanied by the similar material degradation; however, it is important to understand that it comes with the geometrical restrictions of the charge transport as cycling progresses. Although the electrodes we investigated were primarily limited by the lithium-ion charge transfer, the electron flow could be a limiting factor for electrodes that use less amount of conducting agents to increase the energy density or for which the active material has low electronic conductivity. Similarly, in those cases, severe electrochemical reaction non-uniformity and material degradation would occur locally due to the current hot spots. Consequently, upon increasing the loading weight and thickness of the electrode, even small changes in the charge-transfer resistance may accelerate the capacity fading owing to the negative feedback between the current concentration and material degradation. Furthermore, it needs to be noted that current hot spots can cause local heating inside the cell and dendrite formation at thick anodes, and, in extreme cases, can also lead to battery explosion. As thick electrodes are likely to be applied in high-energy density devices in the near future, they should be designed with an understanding of safety issues by considering the charge-transfer kinetics of thick electrodes. As a potential solution, for example, different particle size distributions at the top and bottom of electrodes can be used to control the overall reaction homogeneity or the application of a hierarchical structure would enable relatively facile charge transfer of the electrode. We believe that this study on the capacity fading mechanism of thick electrodes provides useful guidelines to resolve the issues facing high-loading electrodes and to contribute to further development of practical high-energy-density batteries.

Declaration of competing interest

The authors declare that they have no known competing financial interests or personal relationships that could have appeared to influence the work reported in this paper.

CRediT authorship contribution statement

Kyu-Young Park: Writing - original draft, Conceptualization, Methodology, Investigation, Writing - review & editing. **Ji-Won Park:** Writing - original draft, Conceptualization, Methodology, Investigation,

Writing - review & editing. **Won Mo Seong:** Writing - original draft, Data curation, Formal analysis. **Kyungho Yoon:** Methodology, Data curation. **Tae-Hyun Hwang:** Investigation. **Kun-Hee Ko:** Investigation. **Ju-Hyeong Han:** Investigation, Resources. **Yang Jaedong:** Investigation, Resources. **Kisuk Kang:** Supervision, Writing - original draft, Writing - review & editing, Project administration.

Acknowledgements

This work was supported by Project Code (IBS-R006-A2). This work was also supported by the Samsung SDI.

Appendix A. Supplementary data

Supplementary data to this article can be found online at https://doi.org/10.1016/j.jpowsour.2020.228369.

References

[1] M. Armand, J.M. Tarascon, Nature 451 (2008) 652.
[2] Y. Kuang, C. Chen, D. Kirsch, L. Hu, Adv. Energy Mater. 9 (2019) 1901457.
[3] W. Liu, P. Oh, X. Liu, M.-J. Lee, W. Cho, S. Chae, Y. Kim, J. Cho, Angew. Chem. Int. Ed. 54 (2015) 4440–4457.
[4] Y.-K. Sun, S.-T. Myung, B.-C. Park, J. Prakash, I. Belharouak, K. Amine, Nat. Mater. 8 (2009) 320.
[5] M. Sathiya, G. Rousse, K. Ramesha, C.P. Laisa, H. Vezin, M.T. Sougrati, M. L. Doublet, D. Foix, D. Gonbeau, W. Walker, A.S. Prakash, M. Ben Hassine, L. Dupont, J.M. Tarascon, Nat. Mater. 12 (2013) 827.
[6] B. Qiu, M. Zhang, L. Wu, J. Wang, Y. Xia, D. Qian, H. Liu, S. Hy, Y. Chen, K. An, Y. Zhu, Z. Liu, Y.S. Meng, Nat. Commun. 7 (2016) 12108.
[7] S.J. Dillon, K. Sun, Curr. Opin. Solid State Mater. Sci. 16 (2012) 153–162.
[8] S.-H. Park, P.J. King, R. Tian, C.S. Boland, J. Coelho, C. Zhang, P. McBean, N. McEvoy, M.P. Kremer, D. Daly, J.N. Coleman, V. Nicolosi, Nat. Energy 4 (2019) 560–567.
[9] J. Liu, Z. Bao, Y. Cui, E.J. Dufek, J.B. Goodenough, P. Khalifah, Q. Li, B.Y. Liaw, P. Liu, A. Manthiram, Y.S. Meng, V.R. Subramanian, M.F. Toney, V. V. Viswanathan, M.S. Whittingham, J. Xiao, W. Xu, J. Yang, X.-Q. Yang, J.-G. Zhang, Nat. Energy 4 (2019) 180–186.
[10] J.S. Sander, R.M. Erb, L. Li, A. Gurijala, Y.M. Chiang, Nat. Energy 1 (2016) 16099.
[11] M. Singh, J. Kaiser, H. Hahn, J. Electrochem. Soc. 162 (2015) A1196–A1201.
[12] B.-S. Lee, Z. Wu, V. Petrova, X. Xing, H.-D. Lim, H. Liu, P. Liu, J. Electrochem. Soc. 165 (2018) A525–A533.
[13] H. Zheng, J. Li, X. Song, G. Liu, V.S. Battaglia, Electrochim. Acta 71 (2012) 258–265.
[14] Z. Du, D.L. Wood, C. Daniel, S. Kalnaus, J. Li, J. Appl. Electrochem. 47 (2017) 405–415.
[15] K. Kitada, H. Murayama, K. Fukuda, H. Arai, Y. Uchimoto, Z. Ogumi, E. Matsubara, J. Power Sources 301 (2016) 11–17.
[16] J. Newman, J. Electrochem. Soc. 142 (1995) 97–101.
[17] C.-J. Bae, C.K. Erdonmez, J.W. Halloran, Y.-M. Chiang, Adv. Mater. 25 (2013) 1254–1258.
[18] P. Smyrek, J. Pröll, H. Seifert, W. Pfleging, J. Electrochem. Soc. 163 (2016) A19–A26.
[19] K. Evanoff, J. Khan, A.A. Balandin, A. Magasinski, W.J. Ready, T.F. Fuller, G. Yushin, Adv. Mater. 24 (2012) 533–537.
[20] M. Singh, J. Kaiser, H. Hahn, Batteries 2 (2016) 35.
[21] Y. Li, S. Meyer, J. Lim, S.C. Lee, W.E. Gent, S. Marchesini, H. Krishnan, T. Tyliszczak, D. Shapiro, A.L.D. Kilcoyne, W.C. Chueh, Adv. Mater. 27 (2015) 6591–6597.
[22] G. Sun, T. Sui, B. Song, H. Zheng, L. Lu, A.M. Korsunsky, Extreme Mech. Lett. 9 (2016) 449–458.
[23] S. Watanabe, M. Kinoshita, T. Hosokawa, K. Morigaki, K. Nakura, J. Power Sources 258 (2014) 210–217.
[24] D.J. Miller, C. Proff, J.G. Wen, D.P. Abraham, J. Bareño, Adv. Energy Mater. 3 (2013) 1098–1103.
[25] H. Liu, M. Wolf, K. Karki, Y.-S. Yu, E.A. Stach, J. Cabana, K.W. Chapman, P. J. Chupas, Nano Lett. 17 (2017) 3452–3457.
[26] D. Aurbach, J. Power Sources 89 (2000) 206–218.
[27] K. Edström, T. Gustafsson, J.O. Thomas, Electrochim. Acta 50 (2004) 397–403.
[28] L. Yang, B. Ravdel, B.L. Lucht, Electrochem. Solid State Lett. 13 (2010) A95–A97.
[29] W.M. Seong, K.-Y. Park, M.H. Lee, S. Moon, K. Oh, H. Park, S. Lee, K. Kang, Energy Environ. Sci. 11 (2018) 970–978.
[30] C.S. Yoon, D.-W. Jun, S.-T. Myung, Y.-K. Sun, ACS Energy Lett 2 (2017) 1150–1155.
[31] S.-K. Jung, H. Gwon, J. Hong, K.-Y. Park, D.-H. Seo, H. Kim, J. Hyun, W. Yang, K. Kang, Adv. Energy Mater. 4 (2014) 1300787.
[32] M. Dixit, B. Markovsky, F. Schipper, D. Aurbach, D.T. Major, J. Phys. Chem. C 121 (2017) 22628–22636.
[33] J.H. Lee, J.K. Hong, D.H. Jang, Y.K. Sun, S.M. Oh, J. Power Sources 89 (2000) 7–14.
[34] W. Lee, S. Muhammad, T. Kim, H. Kim, E. Lee, M. Jeong, S. Son, J.-H. Ryou, W.-S. Yoon, Adv. Energy Mater. 8 (2018) 1701788.